JOURNAL OF ADVANCED MECHANICAL ENGINEERING APPLICATIONS
e-ISSN: 2716-6201

JAMEA

Vol. 5 No. 2 (2024) 40-49
https://publisher.uthm.edu.my/ojs/index.php/jamea

Integration of Theo Jansen Mechanism Quadruped Robot with 5 Degree of Freedom Robotic Arm for Enhanced Motion Control

Shubham Gopinath Chaudhary[1]*, Anish Karki[1], Suhas Dilip Bhamare[1], Subodh Ashok Shirsath[1], Kiran R. Kaware[1]

[1] *Department of Mechanical Engineering,*
Sandip University, Mahiravani, Nashik, Maharashtra, 422213, INDIA

*Corresponding Author: shubhamchaudhary74862@gmail.com
DOI: https://doi.org/10.30880/jamea.2024.05.02.006

Article Info

Received: 9 June 2024
Accepted: 5 November 2024
Available online: 17 December 2024

Keywords

Theo Jansen mechanism, quadruped robot, 5-degree-of-freedom robotic arm, SolidWorks, CAD modelling, static structural analysis, kinematic analysis

Abstract

This paper presents an in-depth analysis of integrating a Theo Jansen mechanism quadruped robot with a 5-degree-of-freedom robotic arm, focusing on static structural and kinematic aspects. Using SolidWorks Simulation software and ABS material, components are analysed under various loads. Results show max stress, max displacement, and max strain values for each component. Gripper shows max stress 15050 kN/m^2, max displacement 2.755 mm, max strain 0.004 under 10 N load, Base shows max stress 310200 N/m^2, max displacement 0.02 mm, max strain 0.00009 under 30 N load. Shoulder, elbow, and wrist links also show distinct characteristics. Chassis under 20 N load shows max stress 2617 N/m^2, max displacement 6 x 10^{-6} mm, max strain 1 x 10^{-6}. Kinematic analysis includes graph of end effector's Linear Displacement, Linear Velocity, and Linear Acceleration with respect to time under a 100 RPM driving shaft speed.

1. Introduction

The integration of robotic systems has become increasingly prevalent in recent years, driven by the need for enhanced motion control and automation in various fields. One of the intriguing mechanisms used in robotics is the Theo Jansen mechanism, inspired by the kinetic sculptures created by Dutch artist Theo Jansen. This mechanism mimics the walking motion of animals and has been applied in the development of legged robots for its efficient and adaptable locomotion.

This paper focuses on the integration of a Theo Jansen mechanism quadruped robot with a 5-degree-of-freedom (DOF) robotic arm, aiming to achieve a more versatile and capable robotic system. The quadruped robot provides mobility and stability, while the robotic arm offers dexterity and manipulation capabilities. The aim is to integrate the two systems to create a robotic platform capable of performing complex tasks that require both mobility and manipulation. To facilitate the integration process, we utilized SolidWorks software for CAD modelling, allowing us to create detailed models of the components and analyze their structural integrity. Additionally, kinematic analysis of the Theo Jansen quadruped robot was conducted to determine the motion parameters of the end effector, ensuring precise control over its movements.

Through this research, the objective is to demonstrate the feasibility and effectiveness of integrating the Theo Jansen mechanism quadruped robot with a 5-DOF robotic arm, showcasing its potential applications in various

fields. The integrated system represents a significant advancement in robotics, offering a versatile platform for performing complex and challenging tasks that require both mobility and manipulation capabilities.

The study by Shunsuke Nansaia et al presents dynamic analysis of a four-legged Theo Jansen mechanism with numerical simulations using MaTX [1]. Jianxu Wu et al conducted a series of dynamic walking simulations and walking experiments with a multi-legged vehicle to testify the simulation results, showing that type-P is superior to type-R in terms of walking speed, stability, and energy efficiency [2]. Research by Shivamanappa G. Desai et al carried out a kinematic analysis and simulation using MATLAB and Linkage 3.0. Optimal design was also performed using Genetic Algorithm (GA) to determine optimum lengths of links [3]. Jianxu Wu et al presented a novel dual degree-of-freedom (DOF) octopod platform with a reconfigurable trunk study in order to enhance terrain mobility [4]. Additionally, the study by Meera Sitharam et al presented analysis for a common class of 2D mechanisms called 1-dof tree decomposable linkages using CayMos software [5]. Research by Chaoran Wei et al proposed a closed-chain passive-locomotion legged platform (CPLP) in kinematic analysis and zero moment point (ZMP) [6]. Ayan Roy et al presented on the development and optimization of a cost-effective robotic arm for biopsy procedures, demonstrating significant improvements in structural accuracy and longevity through Finite Element Analysis (FEA) and design modifications [7]. Lingala Purandhara Sai Santosh et al presented a study on significance of optimizing robotic arm design through Finite Element Analysis (FEA) to enhance cost efficiency, durability, and material usage, making advanced automation more accessible to small industries [8]. Atirav Seth et al Jaiswal designed aiding unmanned ground vehicles (UGVs) and a 6-degree-of-freedom cylindrical manipulator [9]. Taniya Ghosh et al presented a structural analysis of the robotic arm based on Von Mises stress and strain in order to find failure points [10]. Supriya Sahu, B.B. Choudhury, and B.B. Biswal optimized the design of a 6-axis industrial robot by performing vibration analysis [11]. Alessandro Cammarata et al proposed a variable geometry truss manipulator (VGTM). The elastostatic analysis follows a modular approach that fits the robot's modular design, and snake-like robots have the characteristic of adapting to unstructured environments by exploiting their ability to reconfigure their body's shape [12]. Lalit Patnaik et al presented kinematics and dynamics analysis of the Jansen leg mechanism. They proposed a model that is a useful tool for analysis and design of systems based on the Jansen leg mechanism [13]. Martins-Filho et al explore rule-based reasoning for real-time force distribution in quadruped locomotion control. Utilizing input–output linearization and optimal linear control via the KHEOPS system, it efficiently manages force calculation, demonstrating efficacy and adaptability in real-time locomotion control applications [14]. Ao Xian et al research investigates a novel foot trajectory method to optimize contact force on spacecraft surfaces, validated through theoretical, experimental, and microgravity analyses. This innovative design offers potential for versatile on-orbit servicing, integrating adhesion, crawling, and manipulation capabilities seamlessly [15]. Hongji Liua et al research outlines a stable motion control method for humanoid robots, emphasizing foot strength optimization and swing planning to enhance walking stability. Simulation validation showcases feasibility through a quadratic programming-based approach, hinting at future refinements for complex terrains and exploring arm control integration during locomotion [16]. Gang Wang et al present an innovative amphibious bionic legged robot, showcasing optimized joint design and walking leg mechanism. Post-optimization, it exhibits a significant 29.23% increase in stride length, offering guidance for similar robot development through comprehensive performance evaluations in land and water environments [17]. Tran Thanh Tung et collaborated on a paper introducing a tailored 6 DOF robot arm for Vietnam's economic context. Their design, validated using Solidwork software and CNC manufacturing, emphasizes cost-effectiveness and basic functionality, providing insights for similar robotic arm developments and commercial evaluations [18]. The study by Mohd Ashiq et al introduces a wireless mobile robot arm controlled via a wireless PS2 controller. It emphasizes pick-and-place functionality and underwent thorough performance analysis on an Arduino Mega platform, confirming precision, ease of control, and user-friendly attributes for handling hazardous items and remote object manipulation [19]. Theo Jansen built several multi-legged walkers called Strandbeests that move about on the beach powered only by the wind [20].

2. CAD Modelling Components

2.1 Robotic Arm:

The 5-DOF robotic arm was used in order to properly integrate five main components: the base, shoulder (arm 1), elbow (arm 2), wrist (arm 3), and gripper. The base allows the arm to rotate around a vertical axis, providing the first degree of freedom. The base has a diameter of 90 mm and can rotate 360 degrees. Arm 1 (shoulder) is 162 mm long and can move horizontally with the help of a servo attached to the wrist. Arm 2 (elbow) extends 115 mm horizontally from arm 1, providing additional reach. Arm 3 (wrist) adds another dimension of movement, with a length of 46 mm, allowing for vertical and rotational adjustments. The gripper, located at the end of arm 3, is capable of rotation and grasping and manipulating objects. Fig. 1 depicts the assembly drawing of the 5-DOF robotic arm. The drawing shows the assembly of base, shoulder (arm 1), elbow (arm 2), wrist (arm 3), and gripper to form the complete robotic arm.

J. of Advanced Mechanical Engineering Applications Vol. 5 No. 2 (2024) p. 40-49

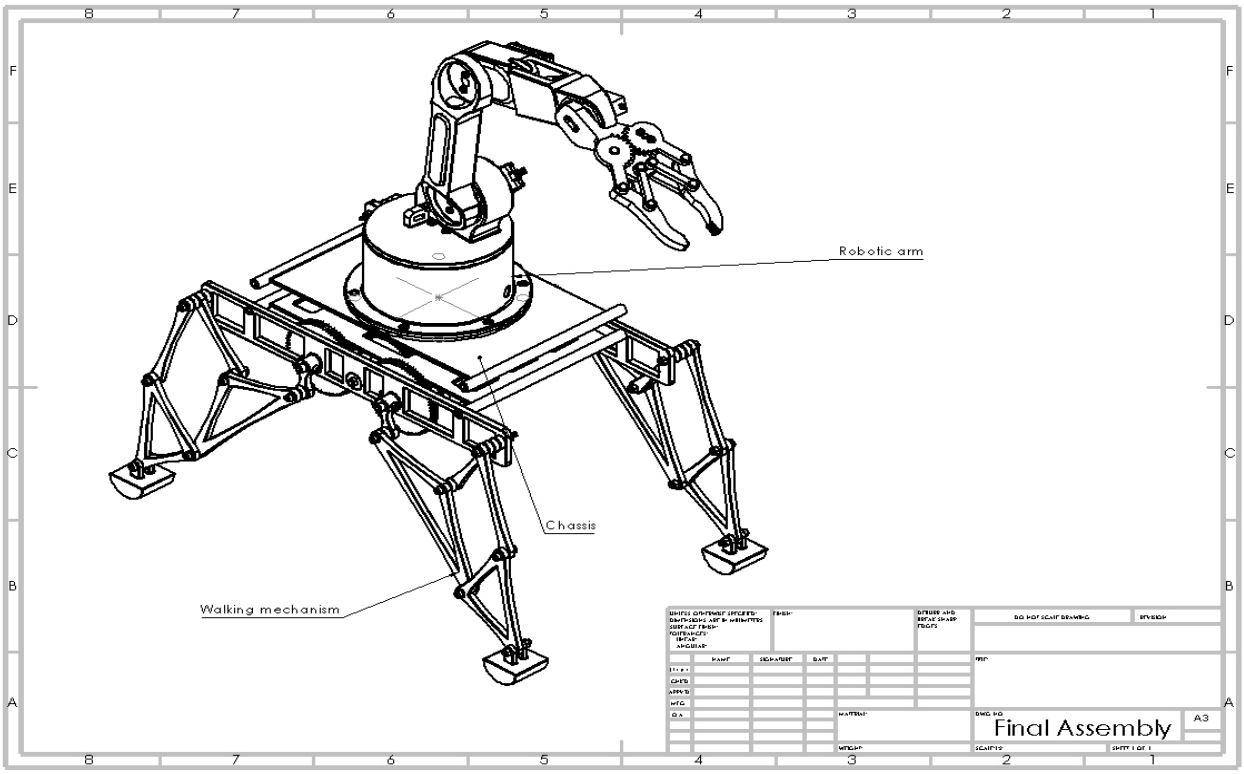

Fig. 1 *Final assembly*

2.2 Chassis

The chassis of the robotic system is designed to provide structural support and house essential components. At the bottom of the chassis, there is a compartment dedicated to housing a DC motor. This motor is connected to a driving shaft, which, in turn, is linked to a 30-tooth gear with module 0.8. This gear mechanism is crucial for transmitting the motor's rotational motion to Theo Jansen based walking mechanism. The motor compartment covered and protected by a walker base plate, which serves as the foundation for the entire robotic assembly. Additionally, there is another plate, referred to as walker base plate 2, which is specifically designed for mounting the 5-degree-of-freedom robotic arm. This plate ensures stability and precision in the arm's movements, allowing it to perform its intended functions effectively. Overall, the chassis plays a vital role in providing the necessary support and structure for the robotic system, enabling it to function optimally. In Fig. 3, the assembly of the chassis is depicted, showing the arrangement and integration of its various components. This includes the placement of the DC motor within its compartment, the connection of the motor to the driving shaft, and the positioning of the 30-tooth gear with a 0.8 module. The assembly also illustrates how the walker base plate covers and protects the motor compartment.

The detailed dimensions of the various components of the chassis are provided, offering specific measurements for each part. These dimensions include the size and shape of the motor compartment, the dimensions of the driving shaft and gear, the dimensions of the walker base plate, and walker base plate 2. These dimensions are crucial for ensuring that each component is accurately manufactured and assembled, contributing to the overall stability and functionality of the robotic system.

2.3 Walking Mechanism

The walking mechanism of the robotic system comprises of a walker base plate with two Theo Jansen mechanism legs attached to either side of the chassis. Two DC motors are used to rotate the driving shafts, which are connected to 30-tooth gears. These gears drive a 60-tooth gear, which, in turn, is connected to a central shaft. The central shaft features two compound gears: a 60-tooth gear that is rotated by the driving shaft gear through mating and a 15-tooth gear that drives two shafts with the help of mating with a 75-tooth gear. These two shafts are known as the long gear shaft and the short gear shaft respectively, which drive the Theo Jansen mechanism legs. This mechanism allows for controlled and synchronized movement of the legs, enabling the robot to walk in a coordinated manner. In Fig. 5, the assembly drawing for the walking mechanism is provided, illustrating how the various components come together to form the functional mechanism. This includes the placement and orientation of the Theo Jansen mechanism legs and the arrangement of the gears and central shaft. The assembly

drawing offers a detailed view of how each part fits into the overall structure, ensuring proper alignment and functionality of the walking mechanism.

2.4 Final Assembly

In the final assembly of the integration of the Theo Jansen mechanism quadruped robot with the 5-degree-of-freedom (DOF) robotic arm, the components are meticulously arranged and connected to ensure optimal functionality. The 5-DOF robotic arm; including the base, shoulder, elbow, wrist, and gripper; is mounted securely on the chassis, which houses the arm's motor, driving shaft, and gear mechanism. The chassis also accommodates the leg mechanism, with the Theo Jansen mechanism legs attached to the sides. The legs are actuated by DC motors and driving shafts, which are linked to gears and a central shaft to enable coordinated movement. The final assembly involves carefully aligning and securing all components, ensuring that they operate smoothly and efficiently. Once assembled, the integrated system is ready to perform complex tasks that leverage the capabilities of both the robotic arm and the Theo Jansen mechanism legs.

3. Static Structural Analysis

Static structural analysis was conducted to assess the structural integrity of the components of the integrated system under various loading conditions. The analysis was performed using finite element analysis (FEA) techniques to simulate the effects of external forces and ensure that the components would not fail during operation.

1. Analysis Setup: component of robot modelled and analyzed using SolidWorks Simulation software.
2. Material Selection: ABS (Acrylonitrile Butadiene Styrene)
3. ABS material: ABS material is an ideal choice for 3D printing a robot due to its strength, durability, and impact resistance, making it suitable for creating robust parts that can withstand wear and tear.

Its ability to withstand higher temperatures compared to PLA makes it suitable for applications where the robot may be exposed to heat or friction. ABS also Provide a degree of flexibility, which can be beneficial for robot designs. Additionally, ABS can be easily post-processed using techniques like sanding, painting, or acetone smoothing to achieve a desired finish or texture. It is readily available and tends to be more affordable compared to other high-performance materials, making it a cost-effective choice for 3D printing projects. The material properties are presented:

- Young's Modulus: 2000 MPa
- Poisson's Ratio: 0.394
- Density: 1020 kg/m3
- Tensile Strength: 3000 MPa
- Yield Strength: 3000 MPa
- Shear modulus: 31890 MPa

4. Robotic Arm

4.1 Robotic Arm Gripper

This section presents the static structural analysis of a gripper component using ABS as the material. The analysis aims to determine the stress, displacement, and strain values under a 10 N load to assess the safety of the gripper design.

Volumetric Properties: Mass: 36.91 gm
Volume: 36911.91 mm^3

Boundary condition and applied load: Fixed boundary conditions were applied to the base of the gripper, and a 10 N load was applied to simulate the gripping action as shown in Fig. 2.

Table 1 *Results from figure 2*

Parameter	Value
Maximum Stress	15050 kN/m^2
Maximum Displacement	2.755 mm
Maximum Strain	4.551 x 10^{-3}

J. of Advanced Mechanical Engineering Applications Vol. 5 No. 2 (2024) p. 40-49

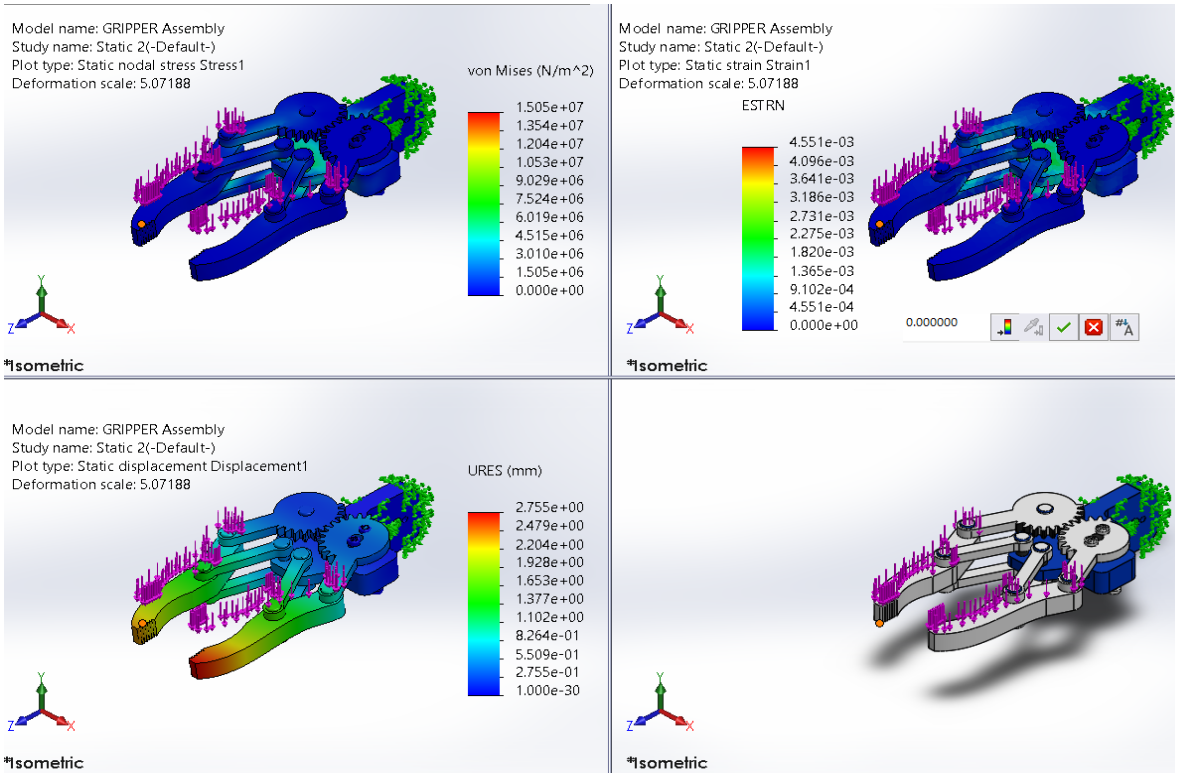

Fig. 2 *Robotic arm gripper result*

4.2 Robotic Arm Base

This section presents the static structural analysis of base component using ABS as the material. The analysis aims to determine the stress, displacement, and strain values under a 30 N load to assess the safety of the base design.

Volumetric Properties: Mass: 167.96 gm
Volume: 164664.28 mm^3

Boundary condition and applied load: Fixed boundary conditions were applied to the bottom of the base, and a 30 N load was applied to simulate the base actions.

Results-Maximum Stress: 3102 MPa
Maximum Displacement: 2.230 x 10^{-2} mm
Maximum Strain: 9.032 x 10^{-5}

4.3 Robotic Arm Shoulder Link (Arm 1)

This section presents the static structural analysis of a shoulder link (arm 1) using ABS as the material. The analysis aims to determine the stress, displacement, and strain values under a 30 N load to assess the safety of the gripper design.

Volumetric Properties: Mass: 61.58 gm
Volume: 61575.80 mm^3

Boundary condition and applied load: Fixed boundary conditions were applied to one corner of shoulder link (arm 1), and a 30 N load was applied to simulate the shoulder link (arm 1) actions (Fig. 3).

Results- Maximum Stress: 8206 MPa
Maximum Displacement: 0.02854 mm
Maximum Strain: 0.0002870

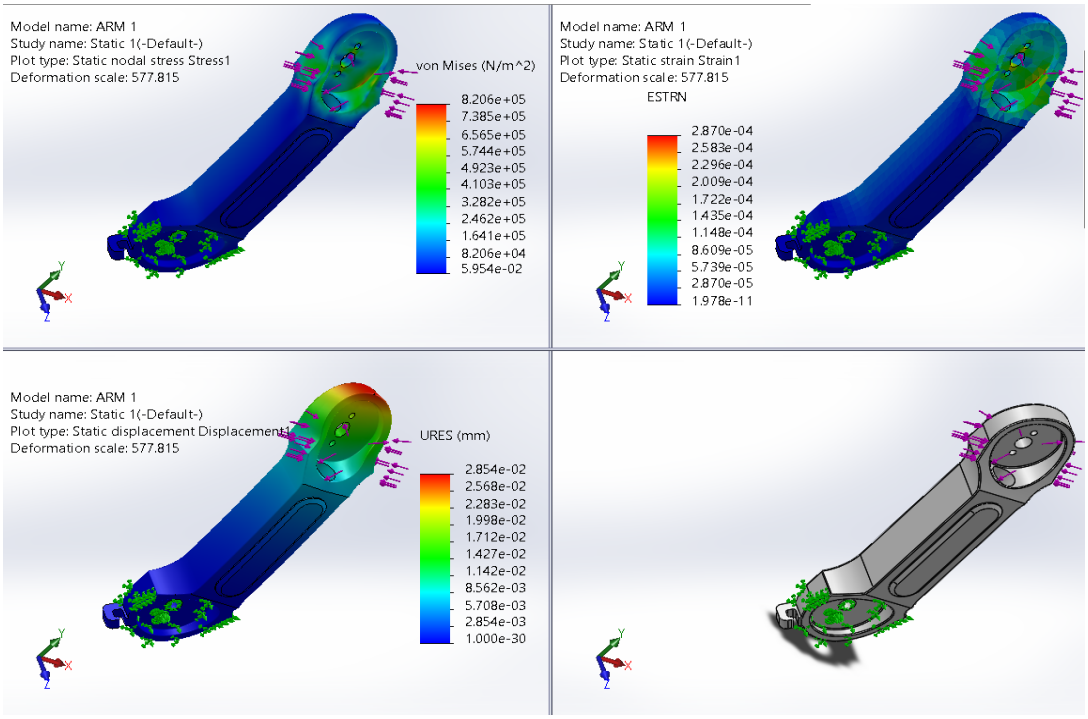

Fig. 3 *Robotic arm shoulder link (arm 1) result*

4.4 Robotic Arm Elbow Link (Arm 2)

This section presents the static structural analysis of an elbow link (arm 2) using ABS as the material. The analysis aims to determine the stress, displacement, and strain values under a 30 N load to assess the safety of the gripper design.

Volumetric Properties: Mass: 55.26 gm
Volume: 55261.84 mm^3

Boundary condition and applied load: Fixed boundary conditions were applied to the one corner of elbow link (arm 2), and a 30 N load was applied to simulate the elbow link (arm 2) actions.

Results- Maximum Stress: 1292 MPa
Maximum Displacement: 0.02680 mm
Maximum Strain: 0.0004747

4.5 Robotic Arm Wrist Link (Arm 3)

This section presents the static structural analysis of a wrist link (arm 3) using ABS as the material. The analysis aims to determine the stress, displacement, and strain values under a 10 N load to assess the safety of the gripper design.

Volumetric Properties: Mass: 17.67 gm
Volume: 17667.21 mm^3

Boundary condition and applied load: Fixed boundary conditions were applied to the one corner of wrist link (arm 3), and a 10 N load was applied to simulate the wrist link (arm 3) actions as shown in Fig. 4

Table 2 *Results from figure 4*

Parameter	Value
Maximum Stress	1518 MPa
Maximum Displacement	2.131 x 10^{-3} mm
Maximum Strain	4.934x 10^{-4}

J. of Advanced Mechanical Engineering Applications Vol. 5 No. 2 (2024) p. 40-49

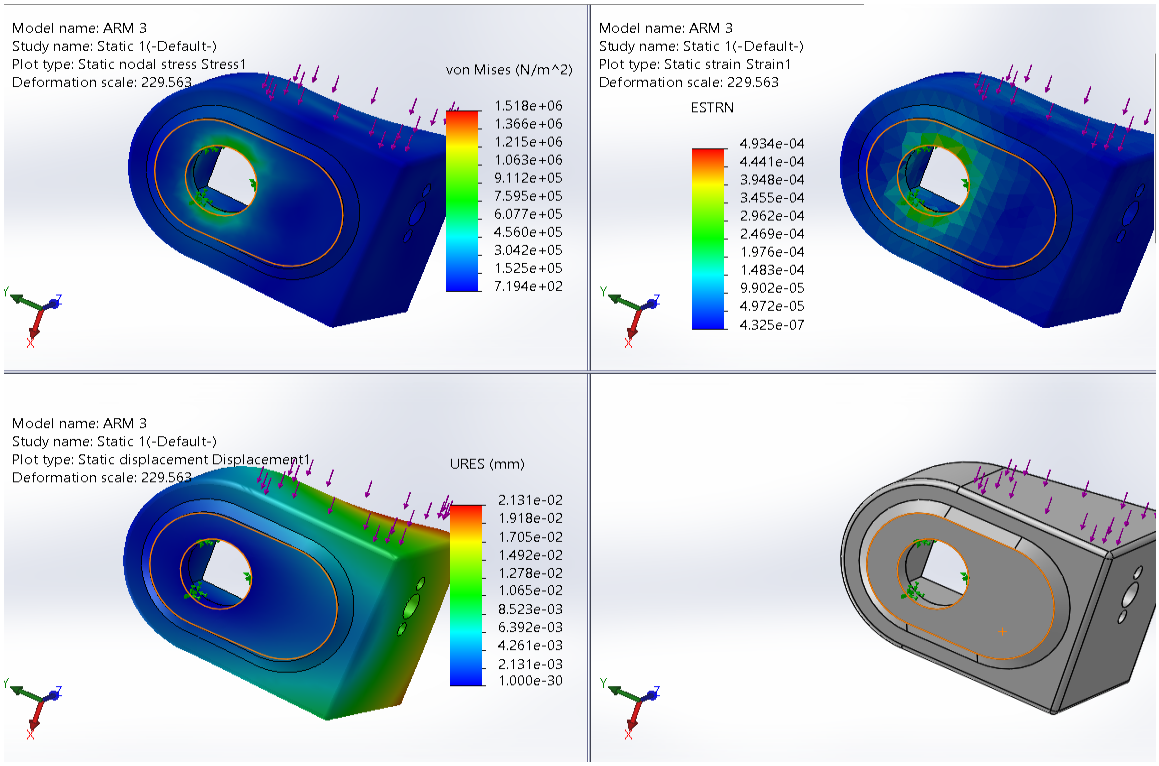

Fig. 4 *Robotic arm wrist link (arm 3) result*

5. Chassis

This Section presents the static structural analysis of a chassis using ABS as the material. The analysis aims to determine the stress, displacement, and strain values under a 20 N load to assess the safety of the chassis design.

Volumetric Properties: Mass: 248.95 gm
Volume: 244594.72 mm^3

Boundary condition and applied load: Fixed boundary conditions were applied to the base of the chassis, and a 20 N load was applied to simulate the chassis action as shown in Fig. 5.

Results- Maximum Stress: 2.617 MPa
Maximum Displacement: 0.000006345 mm
Maximum Strain: 0.000001031

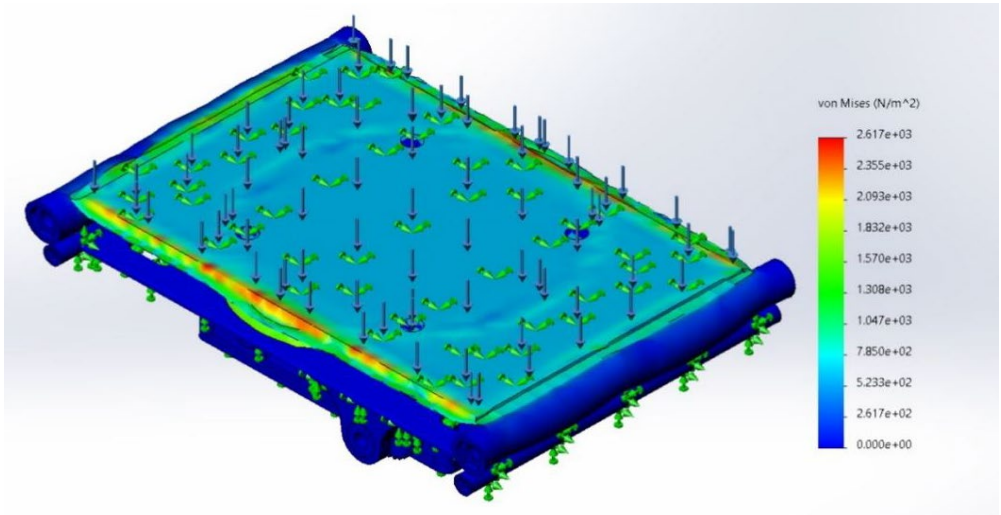

Fig. 5 *Chassis stress result*

6. Kinematic Analysis of Walking Mechanism

In the kinematic analysis of the walking mechanism, a driving shaft speed of 100 rpm was applied to the system in SolidWorks to simulate the movement of the robot. The analysis focused on three key parameters: linear displacement, linear velocity, and linear acceleration magnitude of the end effector.

6.1 Linear Displacement

The graph of linear displacement of the end effector shows the distance travelled by the end effector over time. As the driving shaft rotates at a constant speed, the end effector moves in a periodic motion, mimicking the walking motion of the robot. The displacement graph exhibits a cyclical pattern, with peaks and valleys corresponding to the forward and backward movements of the end effector during each step of the walking motion.

6.2 Linear Velocity

The linear velocity graph illustrates the speed at which the end effector moves along its path. At the beginning of each step, the velocity is low as the end effector starts its motion. As the driving shaft continues to rotate, the velocity increases, reaching a maximum when the end effector is in the middle of its stride. The velocity then decreases as the end effector completes its step and prepares for the next cycle of motion.

6.3 Linear Acceleration Magnitude

The linear acceleration magnitude graph represents the rate of change of velocity of the end effector. It shows how quickly the velocity of the end effector is increasing or decreasing at any given moment. During each step of the walking motion, the acceleration magnitude changes as the end effector accelerates from rest to maximum velocity and then decelerates to rest again.

Fig. 6 presents the motion analysis of the end effector, including linear displacement, linear velocity, and linear acceleration as functions of time.

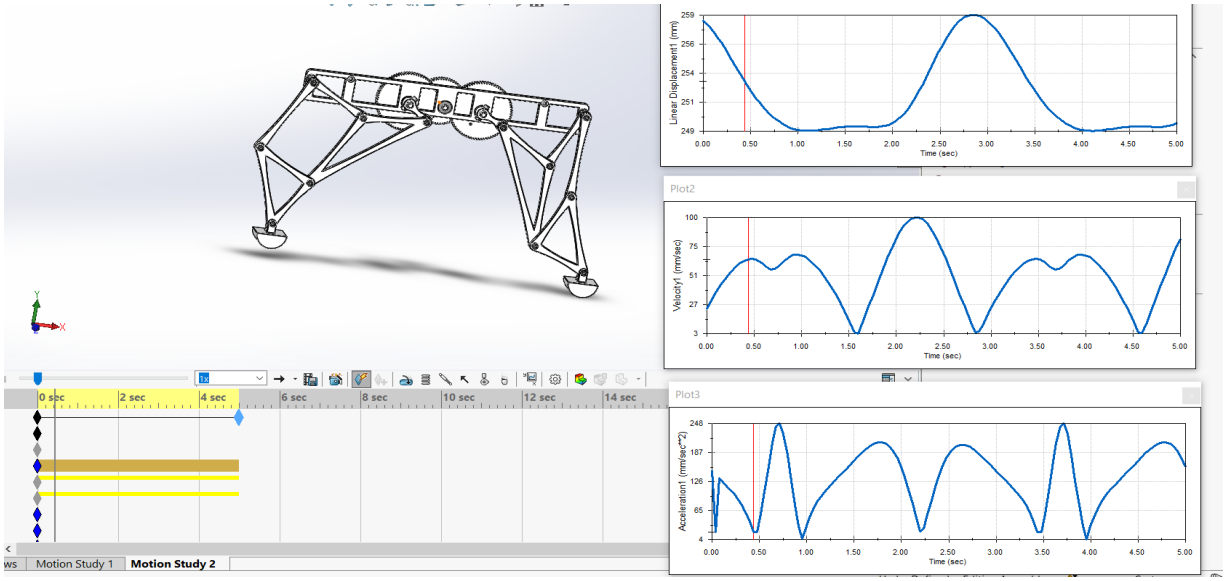

Fig. 6 *Kinematic analysis of walking mechanism*

Table 3 *Motion analysis results*

	Minimum Value	Maximum Value
Linear Displacement	249 mm	258 mm
Linear Velocity	3 mm/s	100 mm/s
Linear Acceleration	4 mm/s^2	248 mm/s^2

7. Results and Discussion

The gripper, being a lightweight component, shows a moderate maximum stress of 15.05 MPa under a load of 10 N. Its relatively high displacement and strain indicate that it undergoes significant deformation under load, suggesting a flexible design. The arm base, a much heavier component, experiences a lower maximum stress despite being subjected to a higher load of 30 N. Its low displacement and strain reflect its rigidity and structural stability. Shoulder link (arm 1) shows higher stress compared to the arm base, indicating its increased susceptibility to deformation under load. However, its displacement and strain are still within a reasonable range for its function. The elbow link (arm 2) experiences the lowest maximum stress among the arm components, with moderate displacement and strain. This suggests a design focused on minimizing stress concentration, likely contributing to the arm's overall durability. The chassis, being the largest and heaviest component, shows minimal stress and negligible displacement and strain. This indicates that the chassis is highly rigid, designed to withstand significant forces without deformation. In the kinematic analysis of the leg components, they are capable of achieving a linear displacement ranging from 249 mm to 258 mm. This significant range of motion suggests that the leg is designed to cover a wide area, making it versatile for tasks that require both short and extended movements. linear velocity of the leg components varies between 3 mm/s and 100 mm/s. This range indicates that the system can perform both slow, controlled movements for precision tasks and faster motions for efficiency in operations that require speed. Additionally, the linear acceleration is between 4 mm/s^2 and 248 mm/s^2. This ability to change speed rapidly is crucial for dynamic applications

8. Conclusion

Based on the given material properties and analysis results, the design of all components, including the gripper, base, shoulder, elbow, and wrist links, as well as the chassis, is considered safe under their respective loads. The maximum stress, displacement, and strain values are within acceptable limits, and they do not exceed the tensile strength or yield strength of ABS (30,000,000 N/m2). Therefore, the robotic arm and chassis design is deemed safe for the specified loading conditions. The kinematic analysis of the leg mechanism demonstrates its ability to achieve the required range of motion and speed for effective locomotion. This analysis is crucial for ensuring that the robot can move efficiently and perform its tasks accurately. Overall, the results of the kinematic and structural analyses suggest that the robotic arm is well-designed and suitable for integration with the Theo Jansen mechanism quadruped robot. This integration could lead to a versatile robotic system capable of complex and coordinated motions for various applications.

Acknowledgement

The authors acknowledge the support and efforts of all the authors of the reference articles and research journals referred to during the drafting of this article.

Conflict of Interest

Authors declare that there is no conflict of interests regarding the publication of the paper.

Author Contribution

Authors confirm contribution to the paper as follows: ***study conception and design:*** *Shubham Gopinath Chaudhary;* ***data collection:*** *Suhas Dilip Bhamare, Anish Karki;* ***analysis and interpretation of results:*** *Shubham Gopinath Chaudhary;* ***draft manuscript preparation:*** *Subodh Ashok Shirsath****; proofreading and similarity checking:*** *Dr. Kiran R. Kaware. All authors reviewed the results and approved the final version of the manuscript****.***

References

[1] Nansai, S., Elara, M. R., & Iwase, M. (2013). Dynamic analysis and modeling of Jansen mechanism. *Procedia Engineering*, *64*, 1562-1571. https://doi.org/10.1016/j.proeng.2013.09.238

[2] Wu, J., & Yao, Y. A. (2018). Design and analysis of a novel walking vehicle based on leg mechanism with variable topologies. *Mechanism and Machine Theory*, *128*, 663-681. https://doi.org/10.1016/j.mechmachtheory.2018.07.008

[3] Desai, S. G., Annigeri, A. R., & TimmanaGouda, A. (2019). Analysis of a new single degree-of-freedom eight link leg mechanism for walking machine. *Mechanism and machine theory*, *140*, 747-764. https://doi.org/10.1016/j.mechmachtheory.2019.06.002

[4] Wu, J., Yang, H., Li, R., Ruan, Q., Yan, S., & Yao, Y. A. (2021). Design and analysis of a novel octopod platform with a reconfigurable trunk. *Mechanism and Machine Theory*, *156*, 104134. https://doi.org/10.1016/j.mechmachtheory.2020.104134

[5] Sitharam, M., & Wang, M. (2014). How the beast really moves: Cayley analysis of mechanism realization spaces using caymos. *Computer-Aided Design*, *46*, 205-210. https://doi.org/10.1016/j.cad.2013.08.033
[6] Wei, C., Sun, H., Liu, R., Yao, Y. A., Wu, J., Liu, Y., & Lu, Y. (2022). Analysis and experiment of thrust-propelled closed-chain legged platform with passive locomotion ability. *Mechanism and Machine Theory*, *167*, 104506. https://doi.org/10.1016/j.mechmachtheory.2021.104506
[7] Roy, A., Ghosh, T., Mishra, R., & Kamlesh, S. S. (2018). Dynamic FEA analysis and optimization of a robotic arm for CT image guided procedures. *Materials Today: Proceedings*, *5*(9), 19270-19276. https://doi.org/10.1016/j.matpr.2018.06.285
[8] Santosh, L. P. S., Mishra, N., Mahanta, S. S. A., Dharmarajan, V., Varma, S. K., & Shoor, S. (2022). Design and analysis of a robotic arm under different loading conditions using FEA simulation. *Materials Today: Proceedings*, *50*, 759-765. https://doi.org/10.1016/j.matpr.2021.05.457
[9] Seth, A., Kuruvilla, J. K., Sharma, S., Duttagupta, J., & Jaiswal, A. (2022). Design and simulation of 6-DOF cylindrical robotic manipulator using finite element analysis. *Materials Today: Proceedings*, *62*, 1521-1525. https://doi.org/10.1016/j.matpr.2022.02.365
[10] Ghosh, T., Roy, A., Mishra, R., & Kamlesh, S. S. (2018). Structural optimization of a CT guided robotic arm based on static analysis. *Materials Today: Proceedings*, *5*(9), 19586-19593. https://doi.org/10.1016/j.matpr.2018.06.321
[11] Sahu, S., Choudhury, B. B., & Biswal, B. B. (2017). A vibration analysis of a 6-axis industrial robot using FEA. *Materials Today: Proceedings*, *4*(2), 2403-2410. https://doi.org/10.1016/j.matpr.2017.02.090
[12] Cammarata, A., Maddio, P. D., Sinatra, R., Tian, Y., Zhao, Y., & Xi, F. (2024). Elastostatic analysis of a module-based shape morphing snake-like robot. *Mechanism and Machine Theory*, *194*, 105580. https://doi.org/10.1016/j.mechmachtheory.2024.105580
[13] Patnaik, L., & Umanand, L. (2016). Kinematics and dynamics of Jansen leg mechanism: A bond graph approach. *Simulation Modelling Practice and Theory*, *60*, 160-169. https://doi.org/10.1016/j.simpat.2015.10.003
[14] Martins-Filho, L. S., & Prajoux, R. (2000). Locomotion control of a four-legged robot embedding real-time reasoning in the force distribution. *Robotics and Autonomous Systems*, *32*(4), 219-235. https://doi.org/10.1016/S0921-8890(99)00128-1
[15] Xiang, A., Zhang, L., & Fan, L. (2024). Design and analysis of an electro-adhesive hexapod robot with convertible limbs in microgravity. *Advances in Space Research*, *73*(3), 1908-1924. https://doi.org/10.1016/j.asr.2023.10.040
[16] Liu, H., Zhu, Z., Sun, Z., Li, Y., Rong, X., Chen, T., & Zhang, G. (2022). Humanoid Biped Robot Locomotion via Quadratic Programming with Compound Constraints. *Procedia Computer Science*, *209*, 67-75. https://doi.org/10.1016/j.procs.2022.10.100
[17] Wang, G., Liu, K., Ma, X., Chen, X., Hu, S., Tang, Q., ... & Han, S. (2023). Optimal design and implementation of an amphibious bionic legged robot. *Ocean Engineering*, *272*, 113823. https://doi.org/10.1016/j.oceaneng.2023.113823
[18] Tung, T. T., Van Tinh, N., Thao, D. T. P., & Minh, T. V. (2023). Development of a prototype 6 degree of freedom robot arm. *Results in Engineering*, *18*, 101049. https://doi.org/10.1016/j.rineng.2023.101049
[19] Yusoff, M. A. K., Samin, R. E., & Ibrahim, B. S. K. (2012). Wireless mobile robotic arm. *Procedia Engineering*, *41*, 1072-1078. https://doi.org/10.1016/j.proeng.2012.07.285
[20] T. Jansen, Strandbeest, https://www.strandbeest.com/, 2014.